# Notch2 signaling guides B cells away from germinal centers towards marginal zone B cell and plasma cell differentiation

T. Babushku[1], S. Rane[2], M. Lechner[1], U. Zimber-Strobl[1#], L. J. Strobl[1*#]

[1] Research Unit of Gene Vectors, Research Group B Cell Development and Activation, Helmholtz Center Munich, German Research Center for Environmental Health GmbH, Feodor-Lynen-Str. 21, D-81377 Munich, Germany.

[2] Irving Institute for Cancer Dynamics, Columbia University, 1190 Amsterdam Ave, New York 10027, USA

* Corresponding author: Lothar J. Strobl, e-mail: lothar.strobl@helmholtz-muenchen.de

[#] these authors contributed equally

**Abstract:** Notch2 signaling has a profound role in driving the development of marginal zone B (MZB) cells. We could show recently that FoB cells act as precursors for MZB cells in mice, however, the mechanism of this differentiation is still elusive. Our current study revealed that Venus expression in CBF:H2B-Venus reporter mice, which is a proxy for Notch signaling, increases progressively with B cell maturation and is highest in MZB cells, suggesting that most peripheral B cells receive a Notch signal and cells with the highest signal preferably develop into MZB cells. Interestingly, Venus expression is heterogeneous in the MZB pool, indicating a loss of Notch signaling over time. Our data also revealed an interplay of antigen induced activation with Notch2 signals, in which FoB cells that turn off the Notch pathway enter GC reactions, whereas B cells with high Notch2 signals undergo MZB and plasmablast differentiation. While Notch2 signaling is dispensable for the initiation of the GC reaction, it supports switching to IgG1$^{+}$ cells in the GC. Integration of our experimental data into a mathematical modelling framework revealed that antigen activation induces a binary cell-fate decision in FoB cells, to differentiate into either GC or MZB cells. The newly generated MZB cells have a short life span and are sustained by influx of antigen activated B cells. Our findings demonstrate that MZB cell generation is a systematic response to TD immunization and provide for the first time a detailed quantitative map of their dynamics during an ongoing TD immune response.

**One-sentence summary:** In antigen-activated FoB cells, ablation of Notch2 does not interfere with GC formation, but obstructs the production of IgG1$^{+}$ GC B cells, whereas induction of Notch2IC inhibits the GC reaction and drives MZB and plasmablast differentiation instead.

## Introduction

Mature splenic B lymphocytes are comprised of two distinct cell populations: Follicular B (FoB) and marginal zone B (MZB) cells, which differ in their immunological function and anatomical localization. FoB cells recirculate between lymphoid organs, whereas MZB cells are mostly sessile in the marginal zone (MZ) and can occasionally migrate between the B cell follicle and the MZ (1, 2). These mature naïve B cells usually remain in a resting state, until they encounter a cognate antigen that triggers their activation. MZB cells respond to T-cell-independent (TI) antigens by proliferation and production of plasma cells (PC) that secrete low-affinity IgM antibodies (3, 4). In contrast, FoB cells respond to T-cell-dependent (TD) antigens, requiring close cell-to-cell contact between activated B and T cells (5-7). Upon activation, FoB cells give rise to intrafollicular structures called germinal centers (GC). Here, they undergo class switching and somatic hypermutation to improve their antigen specificity, resulting in the generation of high-affinity Ig-switched PC and memory B cells (8, 9).

The long-established model suggests that upon rearrangement of their B-cell-receptors (BCR), immature B cells leave the bone marrow and migrate to the spleen as transitional B cells, where they undergo a cell fate decision to differentiate either into FoB or MZB cells (10-14). Nevertheless, it has also been suggested that MZB cells originate from FoB cells, in particular FoB-II cells (15-17). We could recently strengthen this hypothesis by showing that the adoptive transfer of highly purified FoB cells into immunocompetent recipients led to the generation of donor-derived MZB cells via an intermediate MZ precursor stage. Interestingly, the transplanted FoB cells successfully established the physiological ratio of MZB to FoB cells over time (18). Very recently it has been demonstrated that the FoB to MZB transdifferentiation is Notch2-dependent (19). Even though these data provided strong evidence that FoB cells act as precursors for MZB cells, it remained elusive how this differentiation process is controlled.

It has been shown that constitutive active Notch2-signaling in B cells has a strong differentiation-inducing potency, shifting transitional type 1 (T1) B cells and FoB cells towards the MZB cell lineage (18, 20). In contrast, conditional inactivation of Notch2 in B lymphocytes or its ligand Dll-1 in non-hematopoietic cells leads to loss of MZB cells (21, 22). Accordingly, a profound reduction of MZB cells was observed in heterozygous Notch2$^{wt/fl}$//CD19-Cre and Dll-1$^{wt/fl}$//CCL19-Cre mice, indicating a strong dependence of MZB cell development on ligand/receptor dosage. To this end, we conclude that Notch2-signal strength, which may be regulated by the amount of Notch2 receptor expression on the cell surface (21) and its modification by members of the Fringe family (23, 24) as well as the availability of Dll-1-expressing fibroblasts in the B cell follicle (25), regulates MZB cell development. In addition, the interplay between Notch2 and BCR-signaling has been also shown to positively control MZB cell development (10, 13, 26-28). We demonstrated recently that Notch2 cell surface levels are strongly upregulated by BCR-stimulation of murine FoB cells (18). Moreover, research provided by others showed that BCR-signaling induces the recruitment of Adam10 to the plasma membrane and thus enhances the cleavage and subsequent activation of the Notch2-receptor (29). Taken together, these findings imply that BCR signaling acts upstream of Notch2-signaling, resulting in the upregulation of the Notch2-receptor and its downstream activity. Therefore, we had a reason to suspect that B cell activation is a necessary quality of FoB cells, to reach an above-threshold Notch2-signaling activity and to ultimately differentiate into MZB cells.

By studying the Venus expression in different B cell populations of CBF:H2B-Venus Notch-reporter mice, we now demonstrate that almost all B cells receive a Notch-signal under steady-state conditions, and this signal is the strongest in MZB cells. Moreover, we provide evidence that induction of Notch2-signaling upon TD-immunization navigates cells away from the GC

reaction and induces PC and MZB cell differentiation instead, thus making the Notch2 signaling pathway an important binary switch between two opposed B cell fates.

## Results

### All B lymphocytes receive a Notch signal under steady-state conditions

To investigate which B cell populations get a Notch signal, we analyzed B lymphocytes in the bone marrow (BM) and spleen of CBF:H2B-Venus mice (30), which express Venus in all cells that receive a Notch signal. We found that almost all B cell populations in the BM were Venus$^{+}$, with recirculating B cells (CD43$^{-}$B220$^{high}$) having higher Venus expression than pro-B (CD43$^{+}$B220$^{low}$), pre-B and immature B cells (CD43$^{-}$B220$^{low}$). Further subdivision of CD43$^{+}$B220$^{low}$ cells in Hardy's fractions A to C′ revealed that only a minor portion of cells from fractions A and B expressed lower levels of Venus than the remaining developing B cell populations, suggesting that Notch activity starts in very early stages of B cell development (Fig. 1A).

Immature B cells from the BM arrive in the spleen as transitional (T1) B cells (AA4.1$^{+}$B220$^{+}$IgM$^{high}$CD23$^{-}$) and further mature into T2 (AA4.1$^{+}$B220$^{+}$IgM$^{high}$CD23$^{+}$) and T3 (AA4.1$^{+}$B220$^{+}$IgM$^{+}$CD23$^{+}$) cells. T2 B cells can undergo a cell fate decision to become either FoB (AA4.1$^{-}$B220$^{+}$CD23$^{+}$CD21$^{low}$) or MZB cells (AA4.1$^{-}$B220$^{+}$CD23$^{low}$CD21$^{+}$) (10, 11). During B cell maturation in the spleen, Venus expression gradually increased from T1 over T2 to T3 cells, and continued to get higher in FoB and MZB cells. Although Venus expression was the highest in MZB cells, a fraction of them appeared to have lost their Venus signal, suggesting that there are some MZB cells which downregulate or turn off Notch signaling over time (Fig. 1B). This was in accord with our immunohistochemical staining, showing that some MZB cells are indeed Venus$^{-}$ (Fig. 1C).

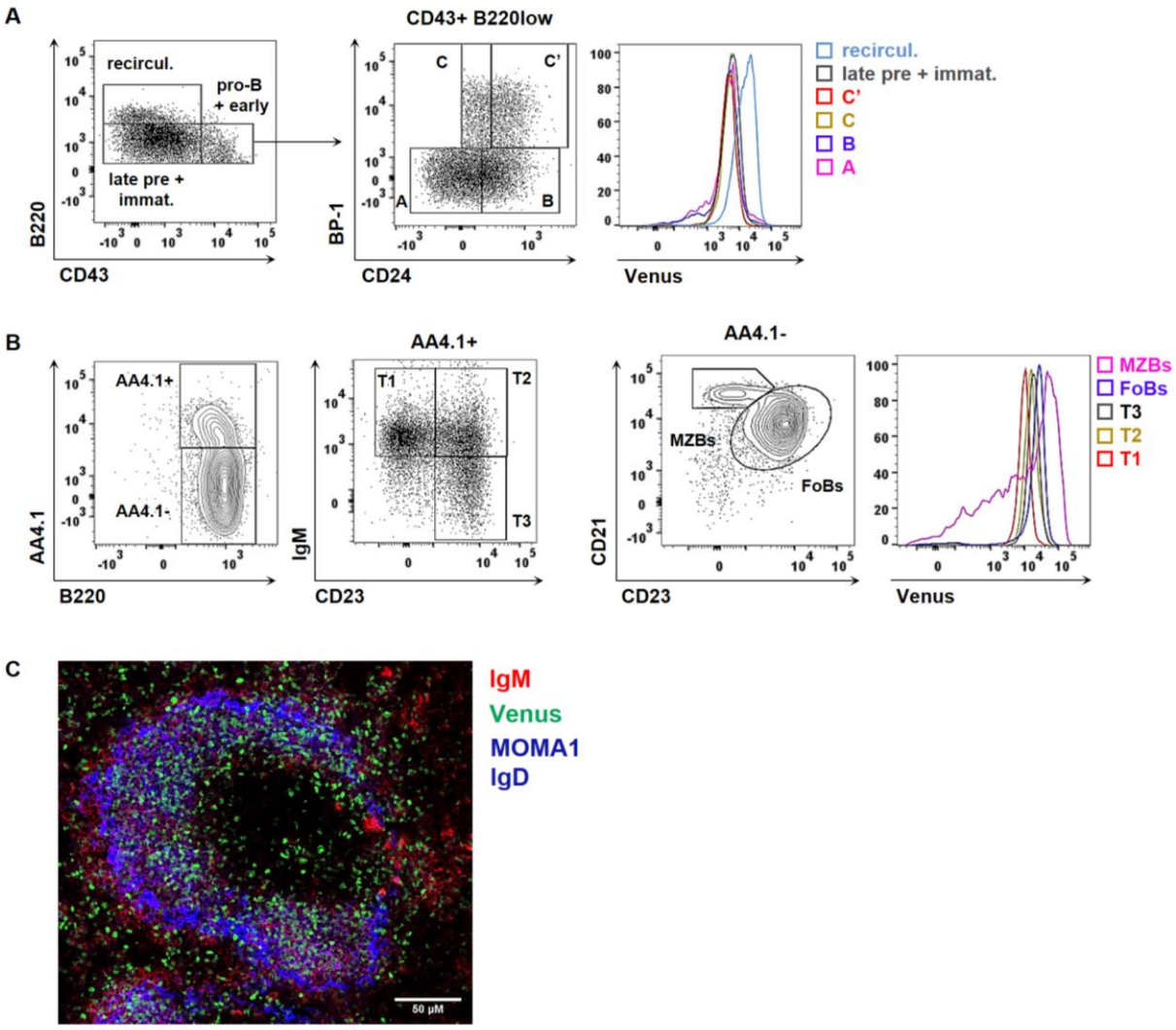


**Fig. 1. All B lymphocytes receive a Notch signal. (A)** Live B220$^{+}$ lymphocytes in the BM of CBF:H2B-Venus mice were subdivided in pro- and early pre- (CD43$^{+}$B220$^{low}$), late pre- and immature (CD43$^{low}$B220$^{low}$) and recirculating (CD43$^{-}$B220$^{high}$) B cells. CD43$^{+}$B220$^{low}$ lymphocytes were further separated into Hardy‘s fractions A-C′ (31). **(A-B)** The histogram overlays show Venus expression in the gated cell populations. n=5. **(B)** Splenic transitional B cells were gated as AA4.1$^{+}$B220$^{+}$ and subdivided into T1-T3 cells according to their CD23/IgM expression. Mature B cells were gated as AA4.1$^{-}$B220$^{+}$ and further separated into FoB (CD23$^{+}$CD21$^{low}$) and MZB cells (CD23$^{low}$CD21$^{high}$). **(C)** Immunofluorescence analysis of splenic sections, stained for MZB cells (IgM$^{+}$, red), FoB cells (IgD$^{+}$; blue) and metallophilic macrophages (MOMA1$^{+}$; blue). Venus-expressing cells (green) are directly visualized without antibody staining. n=3.

**Venus is downregulated in GC B cells, IgG1$^+$ B cells and plasma cells**

To analyze the Venus expression in B cell populations that specifically arise during the primary immune response to a TD antigen, we injected CBF:H2B-Venus mice with 4-Hydroxy-3-nitrophenylacetyl-Chicken Gamma Globulin (NP-CGG) and subsequently analyzed them 7 and 14 days post immunization (p.i.). The Venus signal was progressively downregulated in most germinal center (GC) B cells, compared to non-GC B cells (Fig. 2A). Furthermore, we found that only a small portion of GC B cells was still Venus$^{high}$, with a higher percentage of Venus$^{high}$ cells at day 7 than at day 14 p.i. (Fig. S1A). The immunohistochemical staining for GC B cells was in accordance with our FACS data, showing that the GC structures were mostly Venus$^-$, with only a few Venus-bright GL7$^+$ cells detected. (Fig. 2B). Especially at day 14, the Venus$^{high}$ GC B cells were enriched in the light zone (LZ), whereas Venus$^{mid}$ and Venus$^{neg}$ cells were preferentially found in the dark zone (DZ) (Fig. S1B). We then analyzed the Venus expression in the main outputs of the GC reaction – PCs and IgG1-switched B cells. Venus expression was strongly reduced in splenic TACI$^+$CD138$^+$ PCs (Fig. 2C) and histology for Irf4 -expressing cells re-confirmed this finding (Fig. 2D). Although most PCs had completely shut off the Venus signal, a small portion of TACI$^+$CD138$^+$ cells still showed high Venus expression. A great proportion of these cells also expressed CD19 and B220, suggesting they are (pre-) plasmablasts rather than mature PCs (Fig. 2C). Venus expression was also strongly downregulated in IgG1-switched B cells, both with a GC (CD38$^-$) and non-GC (CD38$^+$) phenotype. However, a fraction of IgG1$^+$ cells showed an intermediate Venus expression, and some CD38$^+$IgG1$^+$ non-GC cells even had high Venus levels. The percentage of CD38$^+$IgG1$^+$Venus$^{high}$ cells increased in the course of the immune reaction (Fig. 2E), suggesting that either some memory B cells receive a Notch signal in the periphery after leaving the GC, or these are the cells which are positively selected in the light zone to leave the GC as switched memory B cells.

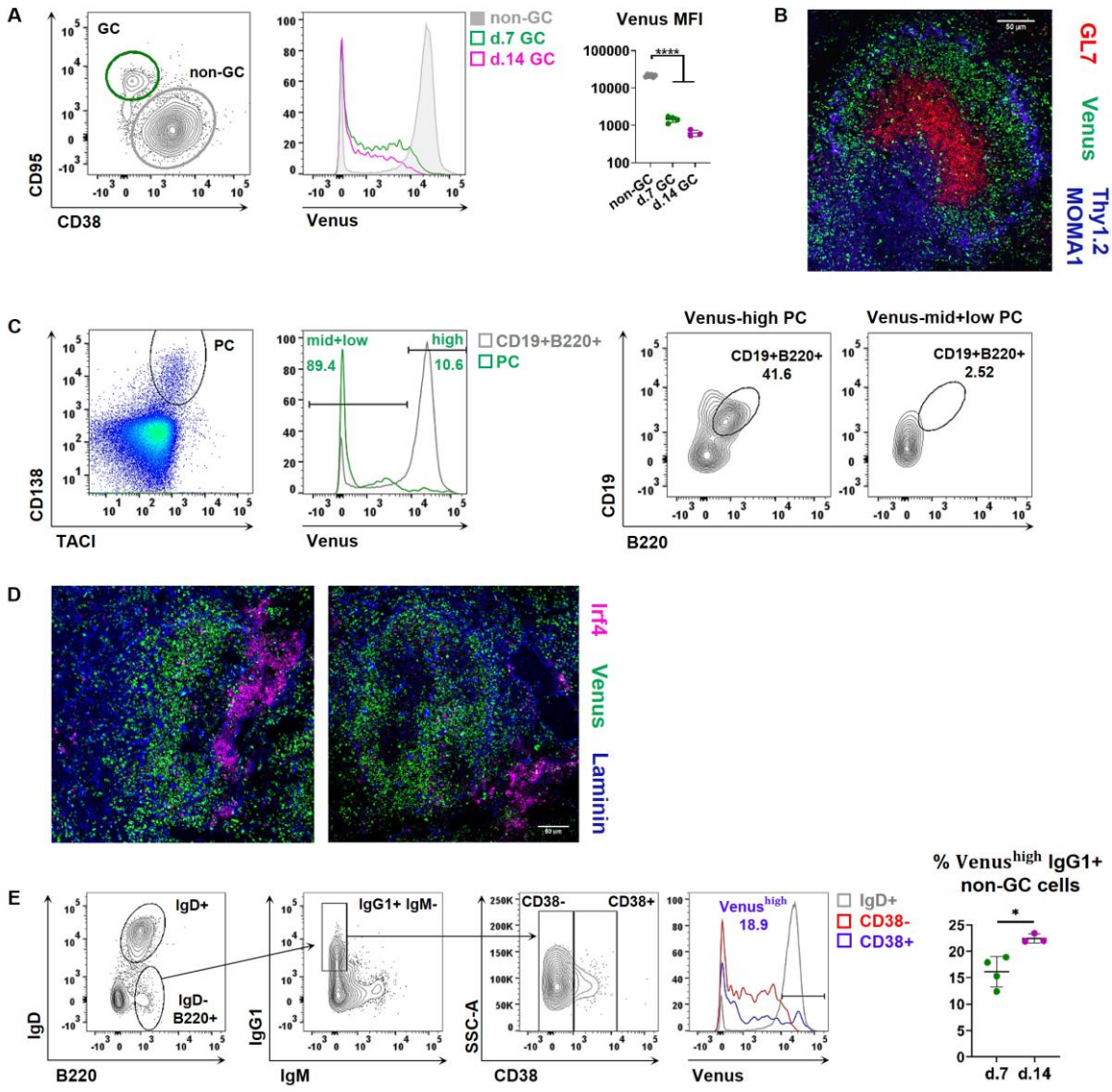


**Fig. 2. Venus is downregulated in most GC B cells, IgG1$^+$ B cells and mature PCs.** FACS plots are pre-gated on live lymphocytes (day 7 p.i.) n≥3. **(A)** The histogram shows an overlay of Venus in GC (CD95$^{high}$CD38$^{low}$) and non-GC B (CD95$^{low}$CD38$^+$) cells. The graph summarizes median fluorescent intensities (MFI) of Venus in the analyzed populations. ****p<0.0001, Tukey's one-way ANOVA of logarithmized MFI values. **(B)** Sections were stained for GCs (GL7$^+$; red), T cells (Thy1.2$^+$; blue) and metalophillic macrophages (MOMA1$^+$; blue) 7 days p.i. Scale bar represents 50 µm. n=2. **(C)** Splenocytes were pre-gated using a large lymphocyte gate and analyzed for PCs (TACI$^+$CD138$^+$). The histogram shows an overlay of Venus expression in PCs and B220$^+$CD19$^+$ B cells, gates and percentages refer to the green histogram of the PCs gated as in the plot. Contour plots depict the CD19/B220 expression in Venus$^{high}$ and Venus$^{mid+low}$ PCs (TACI$^+$CD138$^+$). **(D)** Staining of splenic sections to detect plasmablasts and plasma cells (Irf4$^+$; pink) and basement membranes of endothelial cells (Laminin; blue) 7 days p.i. Scale bar represents 50 µm. n=2. **(E)** Splenic IgG1$^+$ B cells were gated as

$B220^+IgD^-IgM^-IgG1^+$ and further subdivided into GC ($CD38^-$) and non-GC ($CD38^+$) cells. The histogram shows an overlay of Venus in $IgG1^+$ GC and non-GC B cells, compared to $IgD^+$ B cells. The gate and percentage refer to $Venus^{high}$ cells among $IgG1^+CD38^+$ cells. The graph compiles the percentages of $Venus^{high}IgG1^+CD38^+$ non-GC cells. *p=0.017, Welch's unpaired t-test. d7 n=4, d14 n=3.

**Generation of GC B cells is impaired by Notch2IC induction, but not by Notch2 inactivation**

So far, our data revealed that most B cells receive a Notch signal, but Notch signaling is downregulated in the GC. To further study the influence of Notch signaling on the GC reaction, we immunized conditional transgenic mice in combination with the γ1-Cre strain (32), in which the Notch2-receptor is deleted (N2KO//CAR) or constitutively activated (N2IC/hCD2) upon TD immunization with NP-CGG. As controls, we used control/CAR mice, in which the reporter human coxsackie/adenovirus receptor (CAR) is expressed upon Cre-mediated recombination (33). To trace the B cells that successfully underwent Cre-mediated recombination of the loxP-flanked regions, we used the reporter gene CAR in the N2KO//CAR and control/CAR mice, and hCD2 (truncated version of the human CD2) in N2IC/hCD2 mice. The mouse strains are described in Materials and Methods and in Fig. S2A in more detail.

Upon intraperitoneal injection with NP-CGG, the deletion efficiency of the targeted regions was comparable in all mouse strains. $Reporter^+$ B cells in the spleen were detected at day 7 p.i. and their amounts peaked at day 14, followed by a decline to 2% at day 30 (Fig. S2B). Although all mice had similar percentages and kinetics of $reporter^+$ B cells, mice with induced Notch2IC expression were unable to generate GC B cells (Fig. 3A). Thus, only a few GC B cells ($CD38^{low}CD95^{high}$) could be detected in these animals, most of which were $reporter^-$ (Fig. 3B). In addition, immunohistochemistry revealed only small GC structures, which were not localized at the T-/B-cell border in N2IC/hCD2 mice (Fig. 3C). In contrast, N2KO//CAR mice

generated similar amounts of GC B cells like control/CAR animals, which clustered into structures with correct localization inside the splenic follicle (Fig. 3A-C). These data suggest that functional Notch2 signaling is not necessary for GC B cell differentiation, but strong Notch2IC signaling activity interferes with proper GC formation.

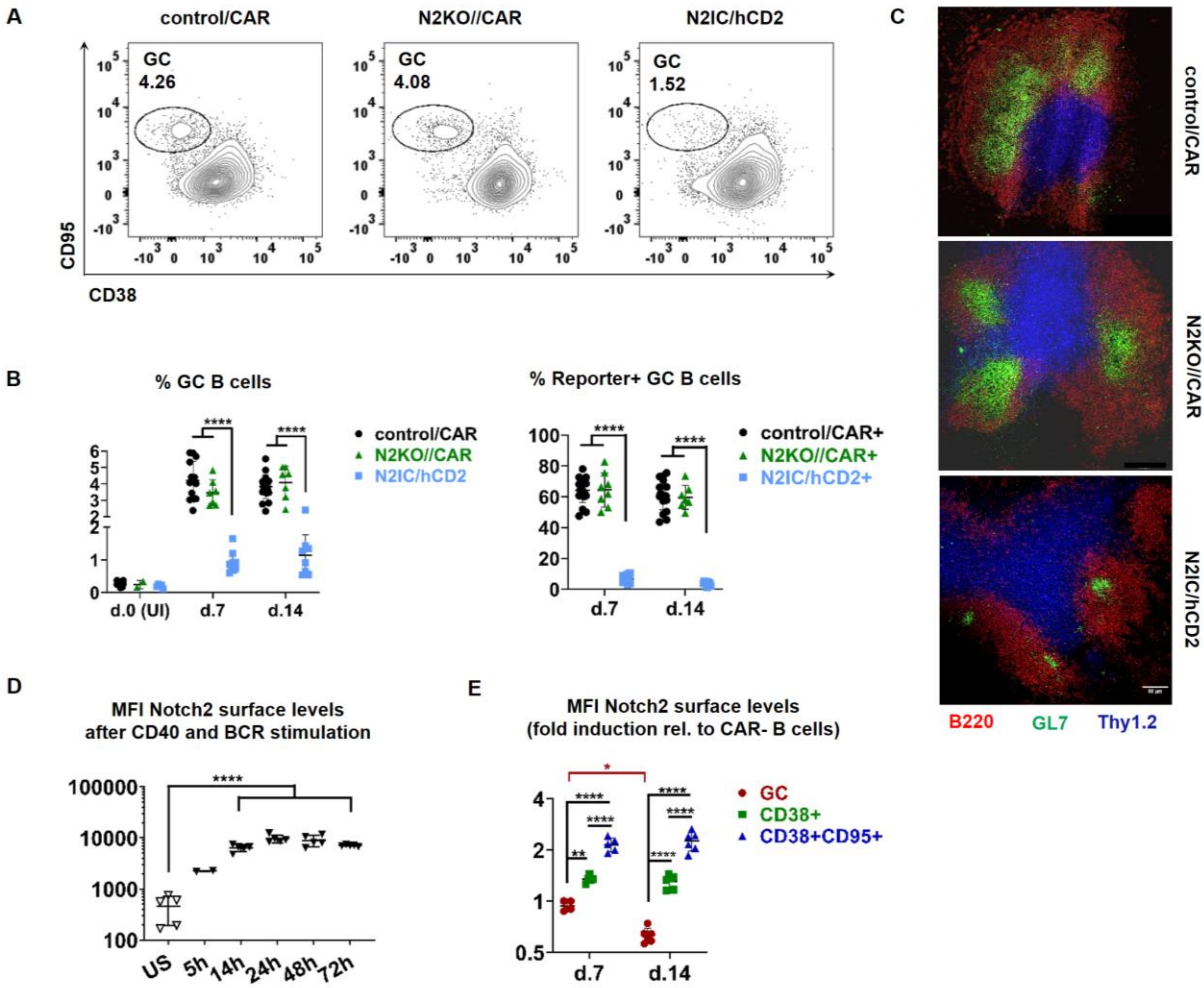


**Fig. 3. Antigen-induced Notch2IC expression inhibits GC formation (A)** Splenic B220$^{+}$ B cells were analyzed for GC B cells (CD95$^{+}$CD38$^{low}$). FACS plots are pre-gated on live lymphocytes and are representative for day 7 p.i.. **(B)** The graph on the left compiles the percentages of total GC B cells in the spleen of mice from the indicated genotypes at the indicated time points p.i.. The graph on the right shows a summary of the percentages of reporter$^{+}$ B cells with a GC B cell phenotype. **(C)** Immunofluorescence analysis of splenic sections from mice of the indicated genotypes 7 days after immunization. Sections were stained for GC cells (GL7$^{+}$; green), B cells (B220$^{+}$; red) and T cells (Thy1.2$^{+}$; blue). Images were obtained with the Leica TCS SP5 II with a HCX PL APO CS 203 objective and LAS AF software. Scale bar represents 50 µm. n=4. **(D)** Graphical summary of median fluorescent intensities (MFI) of Notch2 cell surface expression on purified FoB cells at indicated time points after

α-IgM and α-CD40 stimulation. n=5, except for 5h where n=2. ****p ≤ 0.0001, Tukey's 1-way-ANOVA. **(E)** Fold induction of Notch2 (MFI) in the control/CAR$^+$ CD38/CD95 subpopulations relative to its expression (MFI) in CAR$^-$ B cells. d7 n=5, d14 n=6. *p=0.011, **p=0.001 and ****p≤0.0001, Sidak's 2-way-ANOVA.

**Notch2 surface expression is upregulated on activated FoB cells of control/CAR animals**

Next, we analyzed whether the Notch2 receptor expression on the cell surface varies in different B cell subsets from control/CAR animals. We found a strong upregulation of Notch2 on purified FoB cells upon a combined CD40- and BCR-stimulation in-vitro. This upregulation started early and peaked between 24h and 48h of stimulation (Fig. 3D, S3A). Moreover, we detected a clear upregulation of Notch2 on the surface of reporter$^+$CD38$^+$CD95$^+$ non-GC B cells, while CD38$^-$CD95$^+$ GC B cells progressively downregulated the Notch2 surface levels over time post immunization, in comparison to CAR$^-$ B cells (Fig. 3E, S3B). Thus, our in vitro and in vivo data suggested that Notch2 surface expression is induced on activated non-GC B cells upon CD40- and BCR-engagement, whereas it is downregulated in fully differentiated GC B cells, fitting well with the findings in immunized CBF:H2B-Venus, N2KO//CAR and N2IC/hCD2 mice.

**Inactivation of Notch2 reduces the amounts of IgG1-switched GC B cells**

Since N2KO//CAR mice did not show any impairment in GC B cell differentiation, we analyzed whether lack of Notch2 influences other aspects of the TD immune response. We found that the percentages of splenic reporter$^+$CD138$^+$B220$^-$ PCs were slightly decreased in N2KO//CAR mice compared to control/CAR animals at day 7 p.i., whereas no difference was observed at later time points (Fig. 4A). Moreover, the frequencies of total reporter$^+$IgG1$^+$ B cells were decreased in N2KO//CAR mice, in comparison to controls at day 14 p.i. (Fig. 4B).

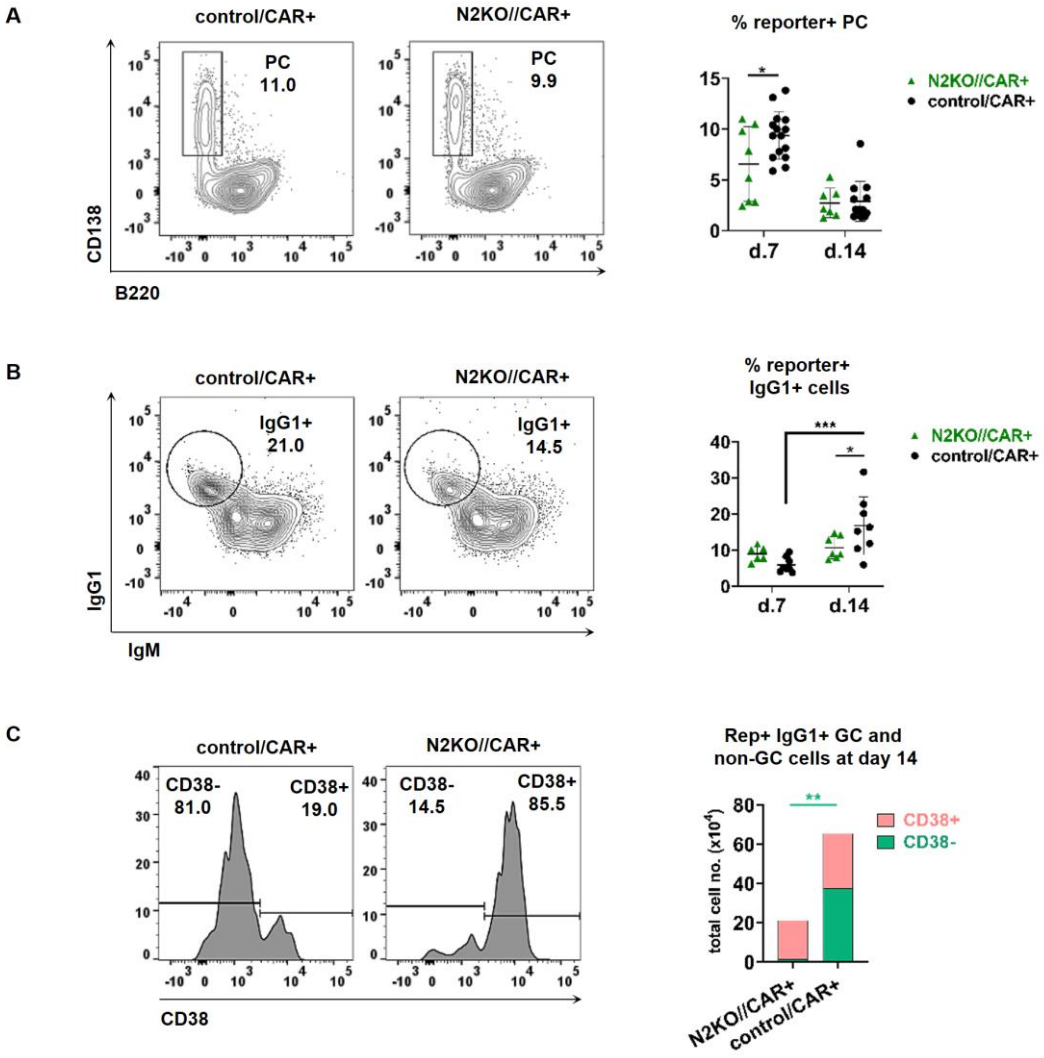


**Fig. 4. Inactivation of Notch2 leads to reduced percentages of IgG1$^+$ GC B cells. (A)** Representative FACS plots for a plasma cells (PCs) staining at day 7 p.i.. Splenocytes were pre-gated using a large lymphocyte gate. Reporter$^+$ cells were analyzed for the differentiation into PCs (B220$^-$CD138$^+$). The graph compiles the percentages of reporter$^+$ PCs at indicated time points. *p=0.024, Sidak's 2-way-ANOVA. n≥7. **(B)** Representative FACS plots from day 14 p.i. to determine reporter$^+$IgG1$^+$IgM$^-$ B cells. The plots are pre-gated on B220$^+$ B cells. The graph compiles the percentages of reporter$^+$IgG1$^+$ cells at the indicated time points. ***p=0.0002, *p=0.040, Sidak's 2-way-ANOVA. **(C)** Reporter$^+$IgG1$^+$IgM$^-$ B cells were separated into GC (CD38$^-$) and non-GC (CD38$^+$) B cells. The stacked bar chart shows the fractions of GC (green) and non-GC (pink) B cells as part of the total IgG1$^+$ B cells in total cell numbers at day 14 p.i. **p < 0.005, Sidak's 2-way-ANOVA.

The observed reduction was due to a strongly diminished proportion of reporter$^{+}$CD38$^{-}$IgG1$^{+}$ GC B cells (Fig. 4C). In sum, our data imply that lack of Notch2 leads to an impaired IgG1 class switch recombination (CSR) in GC B cells during the course of the immune reaction.

**N2IC-expressing cells upregulate Irf4, but fail to induce Bcl6**

Further analysis of the phenotype of N2IC/hCD2$^{+}$ B cells revealed that over 90% of N2IC/hCD2$^{+}$ cells uniformly expressed high CD38 levels, but varied in their CD95 expression (Fig. 5A-B). Intracellular staining for the transcription factors Irf4 and Bcl6, which are key regulators of PC and GC differentiation respectively, revealed an inverse regulation in N2IC/hCD2 and control/CAR mice. Most control/CAR$^{+}$ B cells strongly induced Bcl6 expression, but kept Irf4 levels very low, consistent with their GC B cell phenotype. In contrast, N2IC/hCD2$^{+}$ B cells did not upregulate Bcl6, but showed a strong induction of Irf4 (Fig. 5C). Even though most N2IC/hCD2$^{+}$ cells were Irf4$^{+}$, there was a second fraction, which was Irf4$^{high}$. This fraction was also detected in reporter$^{+}$ cells from control/CAR mice. The Irf4$^{high}$ cells were uniformly B220$^{-}$ in both genotypes (Fig. 5D), pointing to a plasmablast/plasma cell phenotype. The frequencies of B220$^{-}$Irf4$^{high}$ cells were higher in N2IC/hCD2 than in control/CAR mice (Fig. 5E). Immunohistochemistry revealed that the enriched Irf4$^{high}$ cells were predominantly located in the extra follicular regions between neighboring B cell follicles, where plasmablasts (PB) and short-lived PCs are usually located (Fig. 5F).

Together, these findings indicated that N2IC-expression led to the upregulation of Irf4 and prevented the upregulation of Bcl6, thus diverting B cells away from the GC reaction and leading them towards PC differentiation instead.

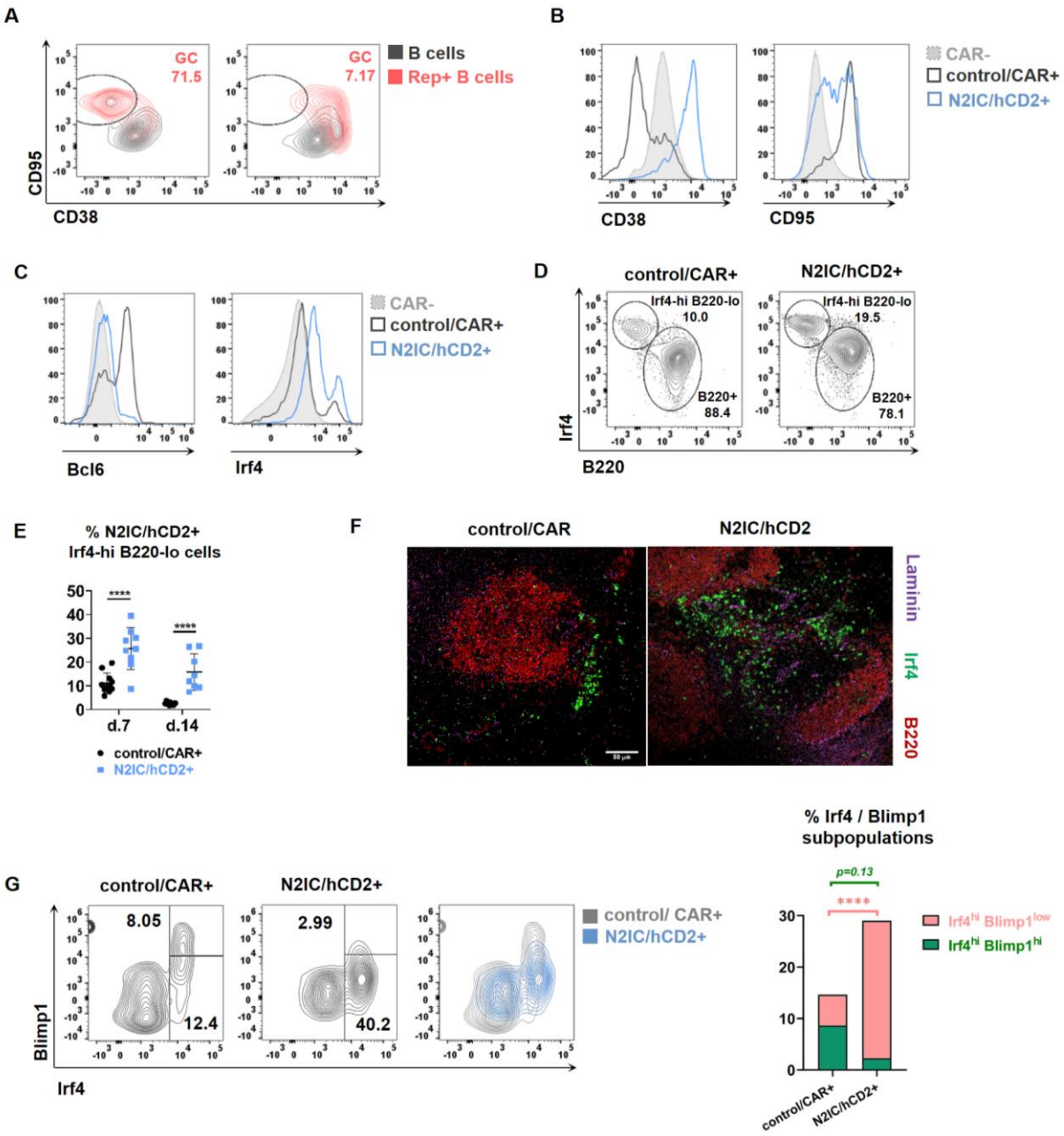


**Fig. 5. N2IC/hCD2$^+$ cells upregulate Irf4, but fail to induce Bcl6.** FACS plots are pre-gated on live lymphocytes (day 7 p.i.). n≥6. **(A)** Splenic reporter$^+$B220$^+$ B cells were analyzed for their GC phenotype (CD95$^+$CD38$^{low}$). Overlays between reporter$^+$ B cells (red) and total B220$^+$ cells (grey) are shown. Gates and percentages refer to the reporter$^+$ population. **(B)** Histograms depict the overlays of CD38 and CD95 expression in reporter$^+$ B cells from N2IC/hCD2 (blue) and control/CAR mice (black), compared to reporter$^-$ B cells (grey). **(C)** Histograms show the overlay of Bcl6 and Irf4 expression in reporter$^+$ lymphocytes (black: control/CAR$^+$, blue: N2IC/hCD2$^+$) and reporter$^-$ lymphocytes (grey). **(D)** Irf4/B220 expression in reporter$^+$ lymphocytes. Two distinct subpopulations were identified: Irf4$^{high}$B220$^{low}$ and Irf4$^{mid}$B220$^+$. **(E)** Summary graph depicting the percentages of reporter$^+$Irf4$^{high}$B220$^{low}$ cells at indicated time points. ****p<0.0001, Sidak's 2-way-ANOVA. **(F)**

Immunofluorescence analysis of splenic sections, stained for (pre-) plasmablasts and plasma cells ($Irf4^{high}$; green) and B cells ($B220^{+}$; red). Scale bar represents 50 µm. n=3. **(G)** The staining was performed after fixation and permeabilization of the cells. FACS plots are pre-gated on live lymphocytes. $Reporter^{+}$ cells were separated into $Blimp1^{high}Irf4^{high}$ mature PCs and $Blimp1^{low}Irf4^{high}$ PB. The overlay shows the Irf4/Blimp1 expression of control/$CAR^{+}$ (grey) and N2IC/$hCD2^{+}$ cells (blue). The stacked bar chart compiles the percentages of $Blimp1^{high}Irf4^{high}$ and $Blimp1^{low}Irf4^{high}$ cells in both genotypes at day 7 p.i. n=5. ****$p<0.0001$, Sidak's 2-way-ANOVA.

## N2IC-expressing cells produce bursts of $IgM^{+}Irf4^{high}Blimp1^{low}$ plasmablasts

To further characterize the differentiation stage of $Irf4^{high}B220^{-}$ cells in N2IC/hCD2 mice, we analyzed the expression of mature PC differentiation factor Blimp1. N2IC-expressing cells showed an attenuated upregulation of Blimp1 in comparison to controls, suggesting that most Notch2IC/$hCD2^{+}Irf4^{high}B220^{-}$cells remained plasmablasts and did not further develop to mature PCs (Fig. 5G). This correlates well with the Venus expression in Notch-reporter mice, in which we detected high levels of Venus in pre-plasmablast and plasmablasts, but a low Venus expression in terminally differentiated PCs. Taken together, our results indicate that Notch-signaling initiates PC differentiation, but has to be turned off to allow for the final stages of PC maturation. Interestingly, ELISpot analysis of the spleen disclosed increased frequencies of NP-specific IgM cells, but strongly reduced NP-specific IgG1 and IgG3 cells in N2IC/hCD2 mice, in comparison to controls at day 7 p.i. (Fig. S4A). A similar trend was visible in the BM, where amounts of NP-specific $IgM^{+}$ cells were increased and the frequencies of $IgG1^{+}$ cells were decreased (Fig. S4B). Taken together, these data suggest that a strong Notch2IC-signal drives cells towards extra follicular plasmablast production, most of which are short-lived ($Blimp1^{low}$), unswitched, IgM-producing cells.

**Some antigen-activated N2IC-expressing B cells differentiate into MZB cells**

In contrast to control animals, IRF4$^{mid}$B220$^{+}$ cells in N2IC/hCD2 mice were clearly Bcl6$^{-}$ and expressed higher levels of Irf4 (Irf4$^{mid}$) (Fig. 6A-B). Considering the role of induced constitutively active Notch2 signaling in the differentiation of FoB into MZB cells under steady-state conditions (18), we suspected that these cells may adopt a MZB cell phenotype over time. Indeed, at day 7 after immunization, a high percentage of N2IC/hCD2$^{+}$Irf4$^{+}$B220$^{+}$ cells had a MZB cell phenotype according to their CD21/CD23 surface expression (Fig. 6C). The amounts of N2IC/hCD2$^{+}$CD21$^{high}$CD23$^{low}$ cells increased with ongoing time after immunization (Fig. 6D, S5). In parallel, these cells also increased their size (FSC) and upregulated IgM, CD1d and CD38 (Fig. 6E), which is fully in accord with the published MZB cell surface phenotype (CD23$^{low}$CD21$^{high}$IgM$^{high}$CD1d$^{high}$CD38$^{high}$). Moreover, the N2IC-expressing cells migrated towards the marginal zone. Some N2IC/hCD2$^{+}$ cells were still located in the middle of the follicle at day 7. However, with ongoing time post immunization, progressively more of these cells were localizing in the MZ (Fig. 6F). By day 30, most of the N2IC/hCD2-expressing cells were at their defined splenic location, forming a MZ ring around the follicle. In sum, our data imply that Notch2IC induction in FoB cells upon TD antigen activation not only caused a shift towards the MZB cell surface phenotype, but also guided the newly generated MZB cells to their correct splenic localization.

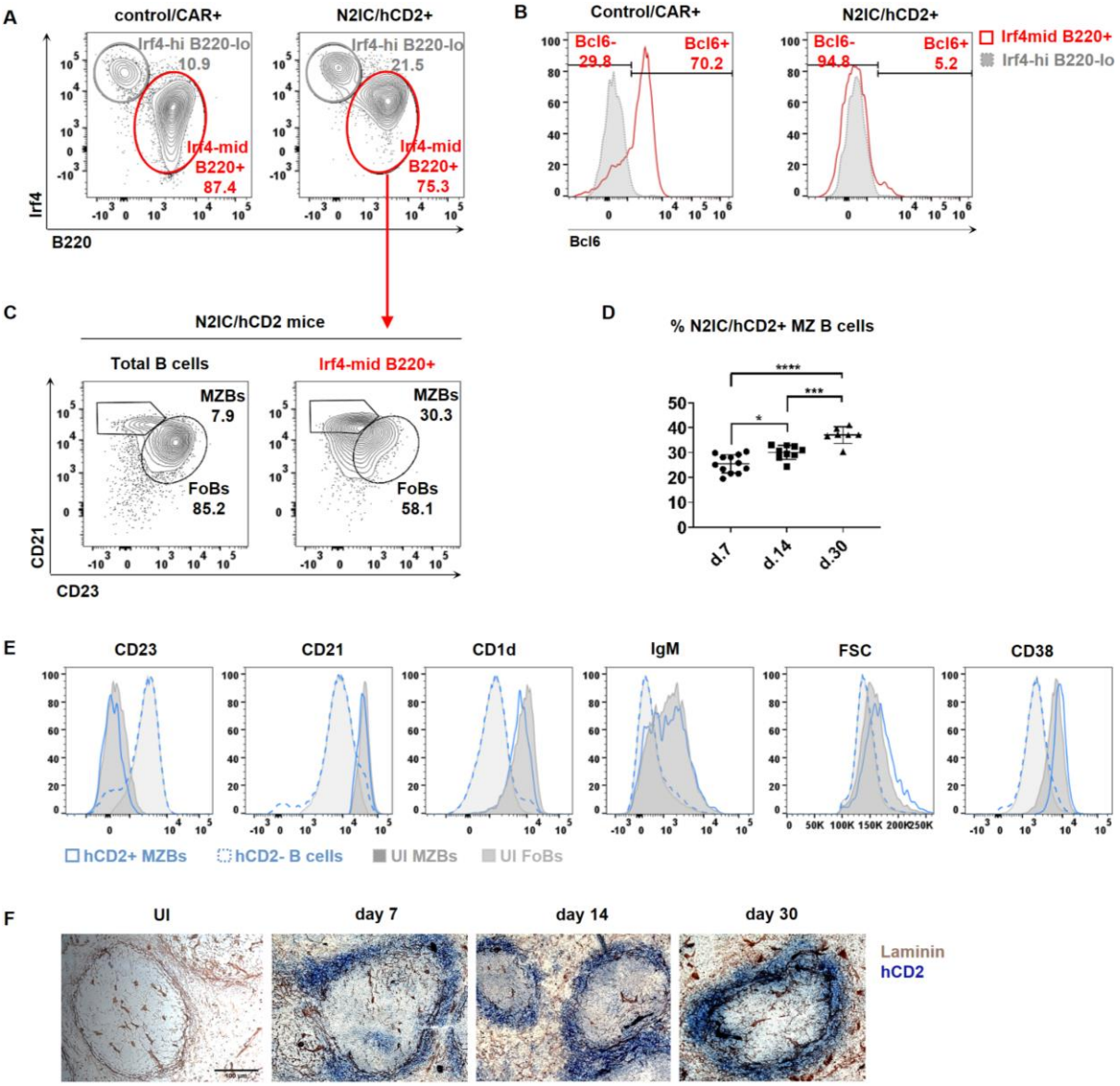


**Fig. 6. N2IC/hCD2⁺ B cells differentiate into MZB cells with proper surface phenotype and splenic localization. (A)** Reporter⁺ lymphocytes were separated into B220$^{low}$IRF4$^{high}$ and B220⁺Irf4$^{mid/low}$ cells. FACS plots are pre-gated on reporter⁺ live lymphocytes. **(B)** Histograms show overlays of Bcl6 expression in reporter⁺B220⁺Irf4$^{mid}$ cells (red) and B220$^{low}$IRF4$^{high}$ PB (grey). **(C)** Gating of MZB (CD21$^{high}$CD23$^{low}$) and FoB (CD23$^{high}$CD21$^{low}$) cells in N2IC/hCD2 mice. The left plot is gated on B220⁺ cells, the right plot is gated on N2IC/hCD2⁺B220⁺Irf4$^{mid}$ cells. **(A-C)** FACS plots are representative for day 7 p.i. n≥4. **(D)** Graphical summary of the percentages of N2IC/hCD2⁺CD21$^{high}$CD23$^{low}$ MZB cells at indicated time points. The gating strategy is shown in figure S5 (d7 n=12, d14 n=9 and d30 n=7). *p=0.023, ***p=0.0003 and ****p<0.0001, Tukey's 1-way-ANOVA. **(E)** Histogram overlays of the expression of indicated markers within N2IC/hCD2⁺ MZB cells and total splenic hCD2⁻ B cells (blue lines) at day 7 p.i., compared to total MZB and FoB cells from unimmunized (UI) N2IC/hCD2 animals (greyscales). n=9. **(F)** Chromogenic

immunohistochemical analysis for the hCD2 expression at the indicated time points. Splenic sections were stained for hCD2 (blue) and for basement membranes of endothelial cells lining the MZ sinus with Laminin (brown). n=3 per time point.

## Generation of cells with a MZ phenotype during the primary immune response is Notch2-dependent

We next asked whether MZB cell differentiation occurs only in the transgenic setting or also physiologically in the course of TD immune responses. To answer this question, we proceeded to analyze control/CAR mice for the appearance of reporter$^{+}$ cells with a MZB cell phenotype upon immunization. Indeed, we found reporter$^{+}$CD23$^{low}$CD21$^{high}$ B cells in the spleen of control/CAR mice. The percentages of these cells gradually increased with ongoing time post injection (Fig. 7), ranging between 2-10% over the total observation period.

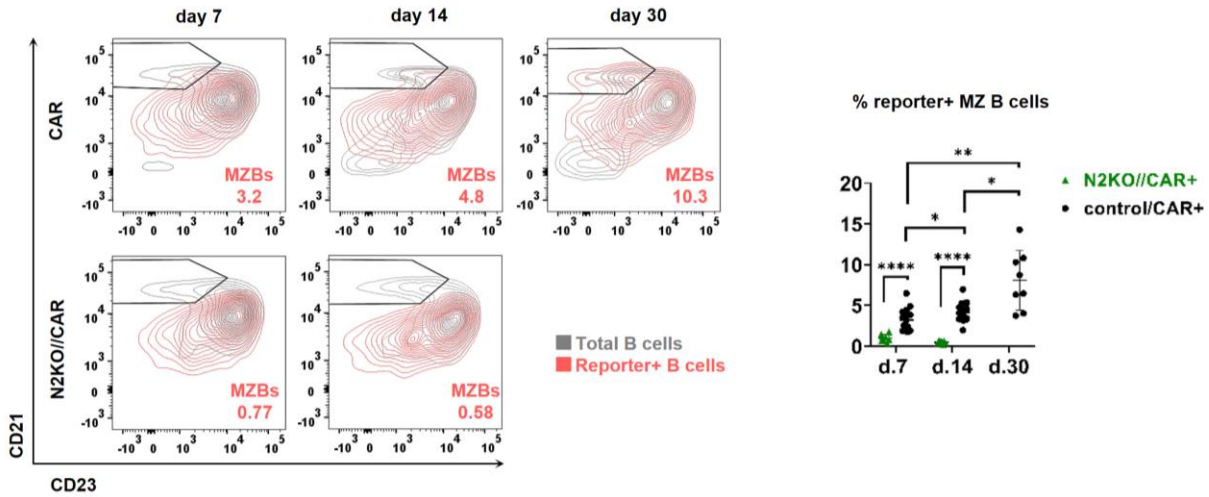


**Fig. 7. Notch2 signaling is necessary for the generation of reporter$^{+}$ cells with a MZB phenotype.** Representative FACS analysis of reporter$^{+}$CD21$^{high}$CD23$^{low}$ MZB cells (red) overlaid with total B220$^{+}$ B cells (grey) in control/CAR and N2KO//CAR mice. The graph summarizes percentages of reporter$^{+}$ MZB cells at the indicated time points. Control/CAR mice: d7 n=16, d14 n=17, d30 n=8; N2KO//CAR mice: d7 n=8, d14 n=7. *p=0.002, **p=0.004, ****p<0.0001, Sidak's 2-way-ANOVA.

Interestingly, reporter$^{+}$CD23$^{low}$CD21$^{high}$ B cells were significantly reduced in immunized N2KO//CAR mice compared to controls, implying that the generation of MZB cells in the

course of the TD immune response is clearly Notch2-dependent (Fig.7). In addition, the newly generated CAR$^+$ MZB cells exhibited high expression of the typical MZB cell surface markers CD1d and IgM, similar to the total MZB cells, but contrary to the FoB cells from control/CAR mice, thus making them completely distinguishable from FoB cells (Fig. S6). Taken together, our results revealed that there is a gradual generation of CAR$^+$ MZB cells over a time course of 4 weeks upon TD immunization. Moreover, we could conclusively show that this process is strongly dependent on functional Notch2-signaling.

**Quantitatively mapping B cell dynamics during an active immune response reveals bifurcation of FoB cells into GC and MZB cell fates**

To define the pathways of recruitment of activated B cells into MZB and GC B cell subsets and to quantify their dynamics during an ongoing immune response, we adopted an integrative strategy that combines data from our immunization experiments with a deterministic mathematical modelling approach. We hypothesized that CAR$^+$ MZB cells emerge either from activated FoB cells (branched pathway) or from cells that have undergone GC reactions (linear pathway) (Fig. 8A). In both these models, we considered that the activation of MZB cells by the TD antigen also contributes to the generation of CAR$^+$ MZB cells (see model details in Fig. S7A-B). Finally, we defined the 'null model', in which all the CAR$^+$ MZB cells are derived purely by the activation of pre-existing MZB cells (Fig. S7C) with no influx from FoB and GC B cells. In the simplest forms of these three models – branched, linear and null – we assumed that GC B cells follow neutral dynamics of birth and death *i.e.* the recruitment of FoB cells into the GC and the net loss of GC B cells (balance between division and true loss by death and differentiation) remain constant over time. Alternatively, the sharp increase in GC B cell numbers and their gradual collapse can also be defined by models in which either the rate of recruitment of FoB cells into GC or the rate of loss of GC B cells varies with time post immunization.

We fitted overall nine mathematical models (3 main models with pathways of MZB cell generation $\times 3$ sub-models capturing GC dynamics) with the time-courses of counts of $CAR^+$ MZB cells, $CAR^+$ GC B cells and total GC B cells from control/CAR mice (red dots in Fig. 8B). Additionally, we used data from N2KO//CAR mice (blue dots in Fig. 8B) in which B cell activation induces Notch2 deficiency and prevents differentiation of $CAR^+$ FoB and GC B cells into a MZB phenotype. In N2KO//CAR mice, the $CAR^+$ fraction in the MZB subset is driven by activation of $CAR^-$ MZB cells and self-renewal of $CAR^+$ MZB cells. We found strongest support for the branched model (table S2), in which activated FoB cells either differentiate into MZB with a constant per capita rate or get recruited into the GC compartment with a time-varying rate. The model predicts rapid turnover of $CAR^+$ MZB cells (mean clonal lifespan < 2 days) (Fig. 8C) and low propensity of MZB cell activation (< 1 in 250 cells, Fig. 8E), suggesting that the $CAR^+$ fraction in MZB subset is largely sustained by the influx of activated FoB cells into the compartment (Fig. 8F, left panel). The total influx of FoB cells into the GC compartment is estimated to be high early on ( ~20% at day 4), which then decreases sharply with time to near 0 by day 10 post immunization (Fig. 8G). In our analysis, the null models with any combination of sub models of GC dynamics failed to capture the dynamics of $CAR^-$ MZB cells (table S2). However, the linear model with time-dependent recruitment of FoB cells into GC showed visually similar fits (dotted lines in Fig. 8B) and comparable parameter estimates (Fig. 8C-G), as that of the best-fitting branched model, despite receiving poorer statistical support (table S2). Perhaps the true model of generation of MZB cells upon immunization lies at the intersection of both branched and linear pathways, in which MZB cells emerge from activated FoB cells early on and are then sustained by differentiation of GC-derived clones into the MZB phenotype in the later stages.

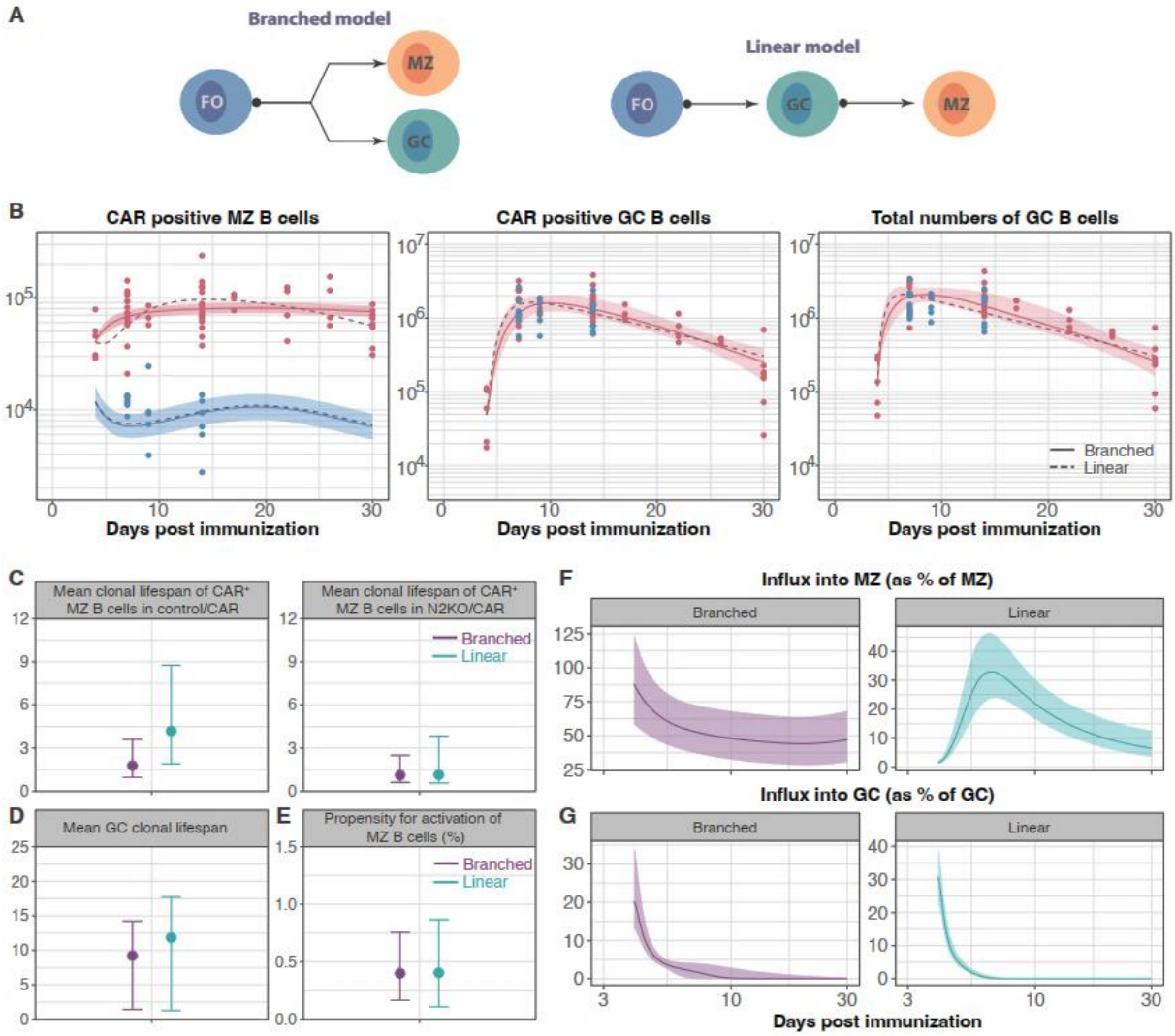


**Fig. 8. Dynamics of CAR$^+$ MZB and GC B cells during a TD immune response. (A)** Schematic of the models depicting B cell fate decisions during an immune response. **(B)** Time-course of counts of CAR$^+$ MZB and CAR$^+$ GC and total GC B cells post immunization in control/CAR (red dots) and N2KO//CAR (blue dots) mice. Fits from the best-fitting branched model with time-dependence in the rate of recruitment of FoB cells into GC reactions (smooth lines) with 95% credible intervals (envelopes). We also show fits from the linear model with time-dependent recruitment, for visual comparison. For clarity, the envelopes around predictions from the linear model are omitted. **(C-G)** Parameter estimates from the branched (purple) and linear (cyan) models with time-dependent recruitment of FoB into GC B cells. **(C-D)** Clonal lifespan is defined as the inverse of 'net loss' rate, which determines the ability of a cell and its progeny to exit the compartment by death and differentiation. **(E)** Rate of activation of CAR$^-$ MZB cells/100 cells. **(F-G)** The total influx of CAR$^+$ cells into MZB subset and FoB cells into GC B cells, plotted as % of total MZB and GC pool sizes, respectively.

## Discussion

The Notch2 ligand Dll-1 is expressed on follicular fibroblasts (25). Therefore, we assume that B cells continuously receive a Notch2-signal in the periphery and the strength of the Notch2-signal determines whether a transitional or a FoB cell differentiates into a MZB cell. To prove our hypothesis, we analyzed the Venus-expression in B cells from Notch-reporter mice (30). We found that both immature and mature B cells are Venus-positive, suggesting that B cells encounter Notch-ligand-expressing cells in the BM, as well as in the periphery. The amount of Venus was gradually increasing throughout stages of B cell development, culminating with the highest Venus level in MZB cells, supporting our view that strong Notch2-signaling is a prerequisite for the development of MZB cells. Surprisingly, a portion of MZB cells downregulated or completely lost the Venus signal, indicating that MZB cells do not receive a *de novo* Notch2-signal in the MZ and therefore lose their Venus-expression with time. By loss of the otherwise high Notch signal, the Venus-low MZB cells may downregulate their Sphingosine-1-phosphate-receptors (S1PR1 and S1PR3), and migrate back into the follicles (1, 18). Indeed, inhibition of Notch2-signaling has been shown to drive MZB cells back into the follicle (34). Alternatively, MZB cells downregulating the Notch-signal could be on the path towards terminal PC differentiation.

Earlier studies revealed that Notch2 signaling interferes with the GC reaction (20, 35), but strongly synergizes with the BCR and CD40 pathways to enhance and sustain B-cell activation (36). This is in line with our observation that (i) Venus expression is strongly and progressively downregulated in GC B cells of CBF:H2B-Venus mice and (ii) Notch2IC/hCD2-expressing B cells cannot enter the GC reaction, but adopt a $CD38^{high}Bcl6^{-}$ non GC phenotype instead. In addition, we found that Notch2-receptor expression is upregulated on activated FoB cells, whereas it is progressively downregulated in GC B cells, suggesting that Notch2 signaling is inversely correlated with GC B cell differentiation.

Although most of the GC B cells were Venus-low and thus devoid of Notch signaling, a small fraction of GC B cells, enriched in the light zone (LZ), still displayed high Venus expression. These cells may be recipients of a Notch-signal during positive selection of GC B cells. It has been demonstrated that follicular dendritic cells express high levels of Notch ligands Dll-1 and Jagged-1, whereas some GC B cells may express Notch1 and Notch2 (37, 38). Our findings that the numbers of $IgG1^+$ GC B cells were strongly decreased in N2KO//CAR mice in comparison to controls suggest that during positive selection of GC B cells, some B cells receive a Notch2 signal which positively influences the generation of $IgG1^+$ cells. In line with this discovery are earlier in vitro studies showing that Notch-signaling through the Dll1-ligand greatly enhances the production of $IgG1^+$ B cells from BCR- and CD40-stimulated FoB cells in vitro (36).

Antigen-induced Notch2IC-expression resulted in the enhanced production of $IRF4^{high}B220^{low}$ cells, which however, had lower amounts of Blimp1 compared with controls, suggesting that PC differentiation is attenuated at the plasmablast stage. This is consistent with higher Venus expression in plasmablasts, than in the terminally differentiated plasma cells, observed in the CBF:H2B-Venus Notch-reporter mice. We conclude from these findings that Notch signaling is necessary to initiate PC differentiation, but has to be turned off during the later stages of PC maturation. It has been suggested earlier that mainly Notch1 positively influences the generation of PC (36). This may explain why the percentages of PCs were only slightly decreased in Notch2-KO mice, whereas Notch2IC, which most likely mimics constitutive active Notch1 and Notch2 signaling, clearly enhanced the entry into PC differentiation.

Lineage tracing of B cells after TD-immunization revealed that a proportion of the antigen-responding cells developed into MZB cells. This process was strongly dependent on Notch2-signaling. Earlier studies already hinted towards an antigen-dependent generation of MZB cells (39-43) and clonally related FoB and MZB cells were identified in rats (44). However, it still

remains unclear whether these MZB cells originate from GC or pre-GC stages. Our mathematical modelling analysis favored the pathway in which MZB cells branch out from activated B cells prior to differentiation into the GC stage. Our data from immunization experiments in Notch2IC/hCD2 and N2KO//CAR mice suggests that this bifurcation is driven by the availability of Notch2-mediated signals. We did not explore a more general model in which both pre-GC and GC B cells differentiate into the MZB phenotype, which remains a strong possibility. In this scenario, the $CAR^+$ MZB compartment would be a mixture of 'classical memory' phenotype B cells with class switched, somatically mutated Igs on their surface and non-mutated, IgM-expressing 'antigen-experienced' cells. This heterogeneity would be apparent in the single cell BCR repertoire composition of the CAR-expressing MZB cells generated upon immunization. Interestingly, these results present a possibility that even at the steady-states, low-level self-antigen induced activation of B cells contributes to continual development of MZB cells.

Our best-fit branched model predicts that CAR expressing MZB cells are short-lived (<2 days), and are largely maintained by the influx from activated B cells. We speculate that the differentiation of CAR-expressing cells into PC phenotype is responsible for their rapid loss from the MZB compartment. Ongoing *Myc* expression and mTOR/Notch2 signaling, which may be highly activated in these cells, has been shown recently to induce rapid division independent PC differentiation of MZB cells (45, 46). It will be interesting to investigate whether the $CAR^+$ MZB cells that are still detectable at later time points after immunization are long-lived MZB cells that are mainly generated from memory B cells. This assumption is supported by earlier studies showing that 8 weeks after immunization, antigen-specific memory B cells are equally distributed between the MZ and follicles (47). Our models also suggest that initial growth of the GC subset is supported by influx from the FoB compartment, which rapidly falls to near zero within a week post immunization. Thereafter, the expansion and

contractions of the initial ‘founder’ clonal families may sustain the compartmental size of GC B cells, which agrees with previous findings (48, 49).

Our new data suggest that the human and murine MZB cell compartment may be more similar than previously suspected. In humans, the MZB cell compartment seems to be heterogeneous and the composition of MZB cells appears to change during life. In children under the age of two, the MZB compartment consists of non-clonal cells with low mutation frequencies. In contrast, in older children and in adults, MZB cells display clonal relationships and are hypermutated suggesting that naïve MZB cells are replaced by antigen-experienced cells during life (50). We postulate that the MZ compartment of young mice strongly resembles that of young children, but may also change during aging and upon immunization. Therefore, it will be interesting to explore in the future, whether the clonal composition and frequencies of hypermutated MZB cells change during aging of mice and whether the ratio of naïve and antigen-experienced MZB cells can be shifted in favor of antigen-experienced MZB cells by sequential TD immunizations.

## Materials and Methods

### Study Design

The objective of this study was to elucidate MZB cell differentiation in mice. We hypothesized that there is an interplay between antigen-induced B cell activation and Notch2 signaling upregulation in the generation of MZB cells during TD immune responses. To examine which B cell types receive a Notch signal in the steady state and upon activation, we analyzed CBF:H2B-Venus reporter mice that express Venus upon Notch signaling. The Venus expression was examined in different resting B cell populations of unimmunized mice, as well as in GC, plasma cells and memory cells of NP-CGG injected mice in FACS and histology. By using conditional Notch2IC-KI and Notch2-KO mice in combination with the GC-specific strain Cγ1-Cre, we followed the fate of transgenic antigen-responding B cells with enhanced or reduced Notch2 signaling in comparison to controls. The primary immune response was monitored by FACS, histology, ELISpot and ELISA at different time points after immunization. In addition, we developed an array of dynamical mathematical models to define and quantify the generation and maintenance MZB and GC cells during an active immune response. Throughout the study, control and mutant mice were age-matched and examined in parallel. Analyses were performed in female and male mice in an unblinded way. All mouse strains were on Balb/c background and analyzed at 10 to 18 weeks of age. Samples sizes and statistical analyses are indicated in figure legends.

**Antibodies used in this study.** The different antibodies used in FACS, ELISA/ELISpot, and histology, their conjugation, clone name, company and the used dilution are listed in Table S1.

## Mice

CBF:H2B-Venus reporter mice (30) were purchased from The Jackson Laboratory, backcrossed into the Balb/c background and further maintained in house. Previously described R26/CAG-CARΔ1$^{StopF}$ (33) and N2IC$^{flSTOP}$ mice (20) were crossbred to the Cγ1-Cre strain (32) to generate R26/CAG-CARΔ1$^{StopF}$//γ1-Cre (control/CAR) and N2IC$^{flSTOP}$//γ1-Cre mice (N2IC/hCD2), respectively. Notch2$^{fl/fl}$ mice (23) were mated to the R26/CAG-CARΔ1$^{StopF}$//γ1-Cre animals to obtain the Notch2$^{fl/fl}$//R26/CAG-CARΔ1$^{StopF}$//Cγ1-Cre (N2KO//CAR) mice. Crossbreeding with the Cγ1-Cre animals resulted in inducible deletion of the lox-P flanked regions in GC and post-GC B cells after antigen injection. The R26/CAG-CARΔ1$^{StopF}$//γ1-Cre reporter mice (control/CAR) were used as age- and sex-matched controls for the N2KO//CAR and N2IC/hCD2 mice. Animals were maintained in specific pathogen-free conditions. Experiments were performed in compliance with the German Animal Welfare Law and were approved by the Institutional Committee on Animal Experimentation and the Government of Upper Bavaria.

## Mouse immunizations

To trigger TD immune responses, 10- to 18- week-old mice were injected intraperitoneally with 100 µg of alum-precipitated 4-hydroxy-3-nitrophenylacetyl (NP)-chicken-gamma-globulin (CCG) (Biosearch Technologies, Novato, CA) in 200 µl sterile PBS (Gibco).

## Cell purification and in vitro cultures

Naïve FoB cells of wildtype Balb/c mice were purified from splenic cell suspension using the MZ and FoB Cell Isolation Kit (Miltenyi Biotech) according to the manufacturer's instructions. Cells were cultured for up to 72 h at a density of $5 \times 10^5$ cells/ml in flat-bottom 96-well plates in RPMI-1640 medium (Gibco), supplemented with 10% fetal calf serum (FCS, PAA Cell Culture Company), 1% L-glutamine, 1% non-essential amino acids, 1% sodium pyruvate and

50 μM β-mercaptoethanol. With the exception of FCS, all supplements were purchased from Gibco. An agonistic antibody against CD40 (2.5 μg/ml; eBioscience HM40-3) and an antibody specific for IgM (15 μg/ml; AffiniPure F(ab′)2 goat anti-mouse IgM, μ-chain, Dianova) was used as a combined stimulus. Cells were harvested at different time points and analyzed by flow cytometry (FACS) after staining with an anti-Notch2-PE antibody. Dead cells were excluded from the analysis by staining them on ice with TO-PRO-3 (Molecular Probes) prior to the FACS analysis.

**Histology**

Murine splenic tissues were embedded in O.C.T. compound (VWR Chemicals, USA), snap frozen and stored at −20 °C. Tissues were sliced with a cryostat with 7 μm thickness, mounted on glass slides and stored at −80 °C for immunohistochemical (IHC) analysis. Chromogenic IHC was performed as described by Lechner et al. (18). Microscopy slides were analyzed using an Axioscope (Zeiss) microscope, equipped with an AxioCam MRc5 digital camera (Carl Zeiss GmbH). For IF staining, air-dried tissue slides were fixed for 10 min with PBS-diluted 3% PFA (Histofix, Carl Roth), rinsed with PBS, and rehydrated for 8 min in PBS + 50 mM $NH_4Cl$. For the staining of the T-/B-cell zone and MZ, splenic sections were blocked with 1% BSA, 5% rat serum, 5% chicken serum in PBS for 30 min, followed by Avidin/Biotin blocking (Vector) according to the manufacturer's protocol. Primary (goat anti-mouse IgM, anti-Thy1.2-Biotin, anti-MOMA1-Biotin), secondary (chicken anti-goat IgG AF647) and fluorophore-coupled antibodies (anti-CD19-APC), as well as Streptavidin-AF594, were incubated for 1 h at room temperature in 0.5% BSA/PBS. For the detection of plasma blasts, tissue sections were permeabilized and blocked with 0.3% Triton X, 1% BSA and 5% goat serum in PBS for 20 minutes. Primary (rat-anti-mouse Irf4, rabbit-anti-mouse Laminin) and secondary antibodies (goat-anti-rat AlexaFluor488 or goat-anti-rat AlexaFluor647, goat-anti-rabbit Cy3) were incubated for 1 h at room temperature in 1% BSA/PBS. Then, directly-coupled antibodies (anti-

mouse B220-APC) were incubated for 2 h at room temperature, where appropriate. For the visualization of germinal centers, sections were blocked with 1% BSA and 5% rat serum in PBS for 30 min. Then, sections were blocked again using the Avidin/Biotin blocking kit. Rat-anti-mouse GL-7-FITC or GL7-APC antibody was incubated overnight at 4˚C, the remaining directly-coupled antibodies (Thy1.2-Biotin, MOMA1-Biotin, B220-APC) and Streptavidin-AlexaFluor594 were incubated for 1 h at room temperature in 1% BSA/PBS. Slides were mounted in ProLong Glass Antifade (Invitrogen). Images were acquired on a TCS SP5 II confocal microscope (Leica) and picture stacks were composed in ImageJ.

**ELISA and ELISpot**

NP-specific antibody titers were measured in ELISA, following the procedure described by Sperling at el., *Blood* 2019 (51). The absorbance was determined with a microplate ELISA reader (Photometer Sunrise RC, Tecan) at an optical density (OD) at 405 nm. For correct quantification of the measured titers internal standards were used, consisting of pooled serums from six to eight NP-CGG immunized mice. All NP-specific titers are given as log10 relative units. For antigen-specific ELISpot with splenic or BM cells, 96-well ELISpot plates (Millipore) were coated overnight at 4°C with NP3– or NP14–bovine serum albumin (BSA; Biosearch Technologies). Subsequent analyzes were performed as previously described by Sperling et al. (51). Spots were visualized and counted with the ImmunoSpot Series 5 UV Analyzer (CTL Europe).

**Flow cytometry (FACS)**

Single cell suspensions were generated from spleen and BM. Surface staining of lymphocytes was performed on ice for 25 min in MACS buffer (Miltenyi). For intracellular FACS staining, cells were fixed with 2% paraformaldehyde (1:2 PBS-diluted Histofix) for 10 min at room temperature and permeabilized in ice-cold 100% methanol for 10 min on ice. Cells were

incubated for 1 h at room temperature with the corresponding antibodies. To include only living cells into the analysis, cells were stained for 5 min on ice with LIVE/DEAD Fixable Blue Dead Cell Stain Kit (Invitrogen) before fixation of the cells. Cytometry analysis was performed on a LSRII FACS Fortessa (BD Biosciences). Results were evaluated using FlowJo (Versions 9 and 10).

**Statistics**

All statistical analyses, including testing for distributions and equal variance, calculations of means and SDs, determining p-values of 1-way or 2-way ANOVA with multiple comparisons tests were done with GraphPad Prism (versions 8 through 10). P values of less than 0.05 were considered significant. *P < 0.05, **P < 0.01, ***P < 0.001, and ****P < 0.0001. Error bars in all figures define means ± SD. The applied statistical analysis test is always indicated in the figure legends. The Prism software was also used to generate all statistical plots.

**Mathematical modelling and statistical analysis**

We developed an array of dynamical mathematical models (detailed in Text S1) and fitted them to the counts of $CAR^+$ MZB, $CAR^+$ GC, and total GC B cells in control/CAR (WT) and N2KO//CAR mice. We used the empirical descriptions of the pool sizes of $CAR^+$ FoB cells and $CAR^-$ MZB cells to define the influx into $CAR^+$ MZB and $CAR^+$ GC compartments (details in Text S2). Models were validated using the Bayesian statistical approach in the programming language *Stan* and predictions were analyzed and plotted in *R*. Leave-One-Out (LOO) cross validation method was used to compare and rank the models (details in Text S3). Code and data used to perform model fitting are freely available at this linked Github repository.

## Supplementary Materials:

**Fig. S1.** Venus expression in light zone (LZ) and dark zone (DZ) splenic GC B cells.

**Fig. S2.** Mouse models for GC-B-cell-specific inactivation or constitutive activation of Notch2.

**Fig. S3.** Notch2 surface expression on purified FoB cells after in-vitro stimulation and on $CAR^+$ CD38/CD95 subpopulations after TD immunization.

**Fig. S4.** NP-specific serum titers and NP-specific plasma cells in the spleen and bone marrow of N2IC/hCD2 and control/CAR mice.

**Fig. S5.** CD23/CD21 staining to separate and quantify MZB cells in N2IC/hCD2 mice.

**Fig. S6.** IgM and CD1d surface phenotyping of $CAR^+$ CD23/CD21 subpopulations of control/CAR animals.

**Fig. S7.** Detailed schematics of the 3 main models with pathways of $reporter^+$ MZB cell generation.

**Fig. S8.** Empirical descriptions of the dynamics of the numbers of FoB and MZB cells.

**Table S1.** List of antibodies used in this study.

**Table S2.** Comparison of models describing population dynamics of MZB and GC B cell populations upon TD immunization.

**Text S1.** Mathematical models of B cell dynamics during a TD immune response.

**Text S2.** Defining phenomenological functions to capture the dynamics of precursor populations for the GC and CAR-expressing MZB cells.

**Text S3.** Model ranking and selection criteria.

**Acknowledgements:** We thank the animal facility of the Helmholtz Center and our animal caretakers for the excellent housing of the mice and Krisztina Zeller for help with genotyping. **Funding:** This work was supported by the Deutsche Forschungsgemeinschaft (DFG ZI1382/4-1). **Authorship Contributions:** T.B. designed, performed and analyzed most experiments. S.R. developed and performed mathematical modelling and wrote the chapter of mathematical modelling and contributed to the final manuscript editing. M.L. performed experiments. L.J.S and U.Z.-S contributed to experimental design and manuscript preparation and data interpretation. T.B., U.Z.-S. and L.J.S wrote the manuscript. All authors read and approved the final paper. **Competing interest:** The authors declare no competing interest.

## References

1. Cinamon G, Zachariah MA, Lam OM, Foss FW, Jr., Cyster JG. Follicular shuttling of marginal zone B cells facilitates antigen transport. Nat Immunol. 2008;9(1):54-62.
2. Arnon TI, Horton RM, Grigorova IL, Cyster JG. Visualization of splenic marginal zone B-cell shuttling and follicular B-cell egress. Nature. 2013;493(7434):684-8.
3. Martin F, Oliver AM, Kearney JF. Marginal zone and B1 B cells unite in the early response against T-independent blood-borne particulate antigens. Immunity. 2001;14(5):617-29.
4. Cerutti A, Cols M, Puga I. Marginal zone B cells: virtues of innate-like antibody-producing lymphocytes. Nat Rev Immunol. 2013;13(2):118-32.
5. Swanson CL, Wilson TJ, Strauch P, Colonna M, Pelanda R, Torres RM. Type I IFN enhances follicular B cell contribution to the T cell-independent antibody response. J Exp Med. 2010;207(7):1485-500.
6. Duchez S, Rodrigues M, Bertrand F, Valitutti S. Reciprocal polarization of T and B cells at the immunological synapse. J Immunol. 2011;187(9):4571-80.
7. Basso K, Klein U, Niu H, Stolovitzky GA, Tu Y, Califano A, et al. Tracking CD40 signaling during germinal center development. Blood. 2004;104(13):4088-96.
8. Paus D, Phan TG, Chan TD, Gardam S, Basten A, Brink R. Antigen recognition strength regulates the choice between extrafollicular plasma cell and germinal center B cell differentiation. J Exp Med. 2006;203(4):1081-91.
9. MacLennan IC, Toellner KM, Cunningham AF, Serre K, Sze DM, Zuniga E, et al. Extrafollicular antibody responses. Immunol Rev. 2003;194:8-18.
10. Pillai S, Cariappa A. The follicular versus marginal zone B lymphocyte cell fate decision. Nat Rev Immunol. 2009;9(11):767-77.
11. Allman D, Lindsley RC, DeMuth W, Rudd K, Shinton SA, Hardy RR. Resolution of three nonproliferative immature splenic B cell subsets reveals multiple selection points during peripheral B cell maturation. J Immunol. 2001;167(12):6834-40.
12. Loder F, Mutschler B, Ray RJ, Paige CJ, Sideras P, Torres R, et al. B cell development in the spleen takes place in discrete steps and is determined by the quality of B cell receptor-derived signals. J Exp Med. 1999;190(1):75-89.

13. Martin F, Kearney JF. Positive selection from newly formed to marginal zone B cells depends on the rate of clonal production, CD19, and btk. Immunity. 2000;12(1):39-49.
14. Pillai S, Cariappa A, Moran ST. Marginal zone B cells. Annu Rev Immunol. 2005;23:161-96.
15. Srivastava B, Quinn WJ, 3rd, Hazard K, Erikson J, Allman D. Characterization of marginal zone B cell precursors. J Exp Med. 2005;202(9):1225-34.
16. Vinuesa CG, Sze DM, Cook MC, Toellner KM, Klaus GG, Ball J, et al. Recirculating and germinal center B cells differentiate into cells responsive to polysaccharide antigens. Eur J Immunol. 2003;33(2):297-305.
17. Agenes F, Freitas AA. Transfer of small resting B cells into immunodeficient hosts results in the selection of a self-renewing activated B cell population. J Exp Med. 1999;189(2):319-30.
18. Lechner M, Engleitner T, Babushku T, Schmidt-Supprian M, Rad R, Strobl LJ, et al. Notch2-mediated plasticity between marginal zone and follicular B cells. Nat Commun. 2021;12(1):1111.
19. Gomez Atria D, Gaudette BT, Londregan J, Kelly S, Perkey E, Allman A, et al. Stromal Notch ligands foster lymphopenia-driven functional plasticity and homeostatic proliferation of naive B cells. J Clin Invest. 2022.
20. Hampel F, Ehrenberg S, Hojer C, Draeseke A, Marschall-Schroter G, Kuhn R, et al. CD19-independent instruction of murine marginal zone B-cell development by constitutive Notch2 signaling. Blood. 2011;118(24):6321-31.
21. Saito T, Chiba S, Ichikawa M, Kunisato A, Asai T, Shimizu K, et al. Notch2 is preferentially expressed in mature B cells and indispensable for marginal zone B lineage development. Immunity. 2003;18(5):675-85.
22. Hozumi K, Negishi N, Suzuki D, Abe N, Sotomaru Y, Tamaoki N, et al. Delta-like 1 is necessary for the generation of marginal zone B cells but not T cells in vivo. Nat Immunol. 2004;5(6):638-44.
23. Besseyrias V, Fiorini E, Strobl LJ, Zimber-Strobl U, Dumortier A, Koch U, et al. Hierarchy of Notch-Delta interactions promoting T cell lineage commitment and maturation. J Exp Med. 2007;204(2):331-43.
24. Tan JB, Xu K, Cretegny K, Visan I, Yuan JS, Egan SE, et al. Lunatic and manic fringe cooperatively enhance marginal zone B cell precursor competition for delta-like 1 in splenic endothelial niches. Immunity. 2009;30(2):254-63.
25. Fasnacht N, Huang HY, Koch U, Favre S, Auderset F, Chai Q, et al. Specific fibroblastic niches in secondary lymphoid organs orchestrate distinct Notch-regulated immune responses. J Exp Med. 2014;211(11):2265-79.
26. Lopes-Carvalho T, Kearney JF. Development and selection of marginal zone B cells. Immunol Rev. 2004;197:192-205.
27. Oliver AM, Martin F, Kearney JF. IgMhighCD21high lymphocytes enriched in the splenic marginal zone generate effector cells more rapidly than the bulk of follicular B cells. J Immunol. 1999;162(12):7198-207.
28. Wen L, Brill-Dashoff J, Shinton SA, Asano M, Hardy RR, Hayakawa K. Evidence of marginal-zone B cell-positive selection in spleen. Immunity. 2005;23(3):297-308.
29. Hammad H, Vanderkerken M, Pouliot P, Deswarte K, Toussaint W, Vergote K, et al. Transitional B cells commit to marginal zone B cell fate by Taok3-mediated surface expression of ADAM10. Nat Immunol. 2017;18(3):313-20.
30. Nowotschin S, Xenopoulos P, Schrode N, Hadjantonakis AK. A bright single-cell resolution live imaging reporter of Notch signaling in the mouse. BMC Dev Biol. 2013;13:15.
31. Hardy RR, Hayakawa K. B cell development pathways. Annu Rev Immunol. 2001;19:595-621.
32. Casola S, Cattoretti G, Uyttersprot N, Koralov SB, Seagal J, Hao Z, et al. Tracking germinal center B cells expressing germ-line immunoglobulin gamma1 transcripts by conditional gene targeting. Proc Natl Acad Sci U S A. 2006;103(19):7396-401.
33. Heger K, Kober M, Riess D, Drees C, de Vries I, Bertossi A, et al. A novel Cre recombinase reporter mouse strain facilitates selective and efficient infection of primary immune cells with adenoviral vectors. Eur J Immunol. 2015;45(6):1614-20.

34. Simonetti G, Carette A, Silva K, Wang H, De Silva NS, Heise N, et al. IRF4 controls the positioning of mature B cells in the lymphoid microenvironments by regulating NOTCH2 expression and activity. J Exp Med. 2013;210(13):2887-902.
35. Valls E, Lobry C, Geng H, Wang L, Cardenas M, Rivas M, et al. BCL6 Antagonizes NOTCH2 to Maintain Survival of Human Follicular Lymphoma Cells. Cancer Discov. 2017;7(5):506-21.
36. Thomas M, Calamito M, Srivastava B, Maillard I, Pear WS, Allman D. Notch activity synergizes with B-cell-receptor and CD40 signaling to enhance B-cell activation. Blood. 2007;109(8):3342-50.
37. Yoon SO, Zhang X, Berner P, Blom B, Choi YS. Notch ligands expressed by follicular dendritic cells protect germinal center B cells from apoptosis. J Immunol. 2009;183(1):352-8.
38. Santos MA, Sarmento LM, Rebelo M, Doce AA, Maillard I, Dumortier A, et al. Notch1 engagement by Delta-like-1 promotes differentiation of B lymphocytes to antibody-secreting cells. Proc Natl Acad Sci U S A. 2007;104(39):15454-9.
39. Liu YJ, Oldfield S, MacLennan IC. Memory B cells in T cell-dependent antibody responses colonize the splenic marginal zones. Eur J Immunol. 1988;18(3):355-62.
40. Shih TA, Roederer M, Nussenzweig MC. Role of antigen receptor affinity in T cell-independent antibody responses in vivo. Nat Immunol. 2002;3(4):399-406.
41. Obukhanych TV, Nussenzweig MC. T-independent type II immune responses generate memory B cells. J Exp Med. 2006;203(2):305-10.
42. Pape KA, Kouskoff V, Nemazee D, Tang HL, Cyster JG, Tze LE, et al. Visualization of the genesis and fate of isotype-switched B cells during a primary immune response. J Exp Med. 2003;197(12):1677-87.
43. White HN, Meng QH. Recruitment of a distinct but related set of VH sequences into the murine CD21hi/CD23- marginal zone B cell repertoire to that seen in the class-switched antibody response. J Immunol. 2012;188(1):287-93.
44. Hendricks J, Visser A, Dammers PM, Burgerhof JGM, Bos NA, Kroese FGM. The formation of mutated IgM memory B cells in rat splenic marginal zones is an antigen dependent process. PLoS One. 2019;14(9):e0220933.
45. Gaudette BT, Roman CJ, Ochoa TA, Gomez Atria D, Jones DD, Siebel CW, et al. Resting innate-like B cells leverage sustained Notch2/mTORC1 signaling to achieve rapid and mitosis-independent plasma cell differentiation. J Clin Invest. 2021;131(20).
46. Limon JJ, Fruman DA. Akt and mTOR in B Cell Activation and Differentiation. Front Immunol. 2012;3:228.
47. Anderson SM, Tomayko MM, Ahuja A, Haberman AM, Shlomchik MJ. New markers for murine memory B cells that define mutated and unmutated subsets. J Exp Med. 2007;204(9):2103-14.
48. Tas JM, Mesin L, Pasqual G, Targ S, Jacobsen JT, Mano YM, et al. Visualizing antibody affinity maturation in germinal centers. Science. 2016;351(6277):1048-54.
49. Meyer-Hermann M, Binder SC, Mesin L, Victora GD. Computer Simulation of Multi-Color Brainbow Staining and Clonal Evolution of B Cells in Germinal Centers. Front Immunol. 2018;9:2020.
50. Kibler A, Budeus B, Homp E, Bronischewski K, Berg V, Sellmann L, et al. Systematic memory B cell archiving and random display shape the human splenic marginal zone throughout life. J Exp Med. 2021;218(4).
51. Sperling SA, Fiedler P, Lechner M, Pollithy A, Ehrenberg S, Schiefer AI, et al. Chronic CD30-signaling in B cells results in lymphomagenesis by driving the expansion of plasmablasts and B1 cells. Blood. 2019.